First direct mass measurement for neutron-rich ^{112}Mo with the new ZD-MRTOF mass spectrograph system

D. S. Hou,[1,2,3,4] A. Takamine,[5,*] M. Rosenbusch,[3,†] W. D. Xian,[6,3] S. Iimura,[5,7] S. D. Chen,[6,3] M. Wada,[3] H. Ishiyama,[5] P. Schury,[3] Z. M. Niu,[8] H. Z. Liang,[9,5] S. X. Yan,[10] P. Doornenbal,[5] Y. Hirayama,[3] Y. Ito,[11] S. Kimura,[5] T. M. Kojima,[5] W. Korten,[12] J. Lee,[6] J. J. Liu,[1,4] Z. Liu,[1,4] S. Michimasa,[13] H. Miyatake,[3] J. Y. Moon,[14] S. Naimi,[5] S. Nishimura,[5] T. Niwase,[3] T. Sonoda,[5] D. Suzuki,[5] Y. X. Watanabe,[3] K. Wimmer,[15,5] and H. Wollnik[16]

[1]*Institute of Modern Physics, Chinese Academy of Sciences, Lanzhou 730000, China*
[2]*School of Nuclear Science and Technology, Lanzhou University, Lanzhou 730000, China*
[3]*Wako Nuclear Science Center, Institute of Particle and Nuclear Studies, High Energy Accelerator Research Organization (KEK), Wako, Saitama 351-0198, Japan*
[4]*University of Chinese Academy of Sciences, Beijing 100049, China*
[5]*RIKEN Nishina Center for Accelerator-Based Science, Wako, Saitama 351-0198, Japan*
[6]*Department of Physics, The University of Hong Kong, Pokfulam, 999077, Hong Kong, China*
[7]*Department of Physics, Graduate School of Science, Osaka University, Osaka 560-0043, Japan*
[8]*School of Physics and Optoelectronic Engineering, Anhui University, Hefei 230601, China*
[9]*Department of Physics, The University of Tokyo, Tokyo 113-0033, Japan*
[10]*Institute of Mass Spectrometry and Atmospheric Environment, Jinan University, Guangzhou 510632, China*
[11]*Advanced Science Research Center, Japan Atomic Energy Agency, Ibaraki 319-1195, Japan*
[12]*IRFU, CEA, University Paris Saclay, F-91191 Gif-sur-Yvette, France*
[13]*Center of Nuclear Study (CNS), The University of Tokyo, Bunkyo 113-0033, Japan*
[14]*Institute for Basic Science, 70, Yuseong-daero 1689-gil, Yusung-gu, Daejeon 305-811, Korea*
[15]*Instituto de Estructura de la Materia, CSIC, E-28006 Madrid, Spain*
[16]*New Mexico State University, Las Cruces, New Mexico 88001, USA*

(Received 3 July 2023; revised 15 September 2023; accepted 25 October 2023; published 27 November 2023)

The atomic masses of ^{111,113}Ag, $^{111–113}$Pd, $^{111–113}$Rh, $^{111–113}$Ru, and ^{111,112}Mo have been measured during the online commissioning experiments of the ZeroDegree multi-reflection time-of-flight Mass Spectrograph (ZD MRTOF-MS) at the RIKEN RI beam factory. The mass of ^{112}Mo has been determined. For the previously known masses, a good agreement between our results and the 2020 Atomic Mass Evaluation has been observed in most cases. The determined two-neutron separation energies for Mo isotopes up to N = 70 show a smooth trend. In this work, the performed experiment and analysis procedure are presented. The theoretical interest in the measured region is highlighted, and the results are discussed in terms of the various mass surface formulas including the new mass data. Furthermore, a comparison between our results and global theoretical mass models is given, and we provide a benchmark for results from a Bayesian machine learning algorithm for future mass extrapolation.

DOI: 10.1103/PhysRevC.108.054312

I. INTRODUCTION

The mass is a fundamental property of the atomic nucleus. High-precision mass measurements of exotic nuclei, by directly determining the nuclear binding energy, play a significant role in studying nuclear structure [1,2] and nucleosynthesis processes [3]. From the nuclear binding energy, the one- or two-neutron separation energy (S_n or S_{2n}) and two-neutron empirical shell gap (δ_{2n}) of the nucleus can be extracted, serving as essential indicators of changes in nuclear structure. High-precision mass data also serve as a critical ingredient for r-process calculations [4], in addition to the half-life data of nuclei (see, e.g., [5]). For the $A = 110$ region, it has been demonstrated that the success of reproducing r abundances depends on the information of shell evolution in the mass models [6,7]. Mass spectrometry technologies have been continuously advanced since the last century [1,8], opening new research fields with increasing precision and accuracy. Nowadays, the multi-reflection time-of-flight mass spectrograph (MRTOF-MS) [9–13], which is an inexpensive and effective device for mass separation and spectrographic analysis of short-lived isotopes, has become one of the primary devices for precise mass measurement worldwide, providing high resolving power in a fast manner [14].

Some theoretical models predict that a harmonic oscillator gap might emerge at $N = 70$, and the classical shell gap

*icot@riken.jp
†marco.rosenbusch@riken.jp

would quench at N = 82 [15–17] in the very neutron-rich region. Experimentally, the γ-ray spectroscopy [7,18,19], lifetime measurements of first 2^+ (2_1^+) states [20], and β-decay half-life measurements [5] in this mass region do not support the appearance of the $N = 70$ shell and the quenching of the $N = 82$ classical shell, despite the fact that the $N = 82$ shell gap at ^{130}Cd is approximately 1 MeV smaller than that at ^{132}Sn [21]. As an additional observable, atomic mass data can provide evidence for shell or subshell closures since the separation energy of nucleons beyond a closed shell or subshell will change significantly. Prior to this work, ^{113}Tc [22] was the most neutron-rich $N = 70$ isotone with an experimentally determined atomic mass.

Below the neutron-rich molybdenum isotopes, a sudden onset of deformation occurs for strontium and zirconium isotopes at $N = 60$ [7,20,23–25]. Recently, the low-Z border of this deformation area has been identified in ^{96}Kr [26,27]. In the Kr isotopic chain, deformation develops more gradually [26,28,29]. In addition, a low-lying state nearby the 2_1^+ state has been identified in ^{98}Kr, indicating shape coexistence, as identified in ^{96,98}Sr [23]. In the Zr isotopic chain, shape coexistence has been observed in ^{98}Zr [30,31], confirming the sudden onset of collectivity at $N = 60$. On the theoretical side, the sudden shape transition and coexistence can be explained by type-II shell evolution [24,32], a result of the interplay of tensor forces and particle-hole configurations. The state-of-the-art beyond-mean-field approaches have been used to reproduce the sudden onset of deformation in this region, and have shown good agreement with experimental results [29]. To study the structural evolution beyond $N = 60$ in the heavier molybdenum isotopes, detailed γ-ray spectroscopy of ^{106,108,110}Mo following β decay was carried out [33]. The results suggested that their ground states are prolate deformed, based on comparison with beyond-mean-field calculations using two kinds of Skyrme interactions. Furthermore, the odd-even energy staggering of levels built on top of the 2_2^+ states suggested a γ-vibrational shape for these bands in ^{106,108,110}Mo. In contrast, a recent theoretical work investigated the shape evolution and shape coexistence in even-even $^{90–116}$Mo using the covariant density functional theory (CDFT) with density-dependent point-coupling parameter sets [34]. The calculations suggested that the ground-state shapes of ^{90,92,94}Mo are spherical, but for $^{96–108}$Mo deformation occurs and manifests as a triaxial shape. Finally, from ^{108}Mo to ^{110}Mo, a further transition from triaxial to oblate shape is indicated in the calculations.

In this work, we report the precise atomic mass measurements of ^{111,113}Ag, $^{111–113}$Pd, $^{111–113}$Rh, $^{111–113}$Ru, ^{111,112}Mo using the new MRTOF-MS system at RIKEN's Radioactive Isotope Beam Factory (RIBF) facility. This is the experimental determination of the atomic mass of $^{112}_{42}$Mo, and confirmation of the atomic mass of ^{112}Rh previously measured [35,36] by the Jyväskylä Penning trap group with large deviation from the expected value. The experimental setup and detailed data analysis procedure will be given in Secs. II and III. The experimental results will be compared with the 2020 Atomic Mass Evaluation (AME2020) [37], and the calculated shape transition for Mo isotopes will be discussed in terms of S_{2n} and δ_{2n} extracted from the new mass data. Furthermore, we compare the mass results in this region with state-of-the-art mass models in Sec. IV, and include our data in calculations using the approach of a Bayesian machine learning (BML) algorithm.

II. EXPERIMENT

The mass measurements were carried out in symbiotic experiments with nondestructive in-beam γ-ray spectroscopy measurements (HiCARI project [38,39]) at the RIBF facility [40,41] of the RIKEN Nishina Center in Japan. The isotopes of interest were produced by in-flight fission of a 345 MeV/nucleon ^{238}U primary beam with an intensity of 60 pnA delivered by RIKEN's superconducting ring cyclotron (SRC) accelerator. A 740 mg/cm^2 ^{9}Be target was used, and the in-flight fission fragments were selected and transported by the BigRIPS Separator [42,43]. A secondary target was employed for in-beam γ-ray spectroscopy measurements (main experiment) for specific nucleon knock-out reactions. Unreacted secondary beam and reaction products from the secondary target were further transported through the ZeroDegree (ZD) spectrometer and available for study with the ZD-MRTOF setup.

The ZD-MRTOF setup behind the ZD spectrometer consists of three main parts: a cryogenic helium gas-filled catcher cell [44,45], an ion trap chamber, and a newly built MRTOF-MS [14,46] (see Fig. 1). The typical energy of the incoming beam was greater than 100 MeV/nucleon downstream of the ZD spectrometer. In order to stop the reaction products in the catcher cell, a flat degrader (1 mm-thick stainless steel) [47] was installed in front of the entrance window of the catcher cell, where the degrader thickness can be adjusted by remote-controlled rotation. The catcher cell system comprises an outer vacuum chamber and a 50 cm-long inner chamber filled with pure helium. The incoming products pass from the ZD beam line into atmosphere via a 125 μm Kapton window, travel through 775 mm of air and then enter the ZD MRTOF's gas catcher cell through an outer Ti window of 50 μm thickness to enter a vacuum region before passing through an inner mylar window of 6 μm thickness to enter the helium environment which serves as the stopping region. The incoming products enter as highly charged, energetic radioactive ions (RI) and are stopped in ionizing collisions with the helium gas. Interactions with the helium gas quickly reduce the RI to a 3+ or 2+ charge state [48], while interactions with gas contaminants such as Ar, N_2, O_2, and H_2O reduce the RI to singly charged ions or neutral atoms. In this commissioning run, the setup allowed for cooling the inner catcher cell chamber down to 180 K by a cryocooler to freeze-out molecular impurities [49], while the vacuum in the outer chamber served as thermal insulation. Despite the cryogenic cooling, the level of gas contaminants in this case was such that most RI were extracted from the gas cell as singly charged ions. A pressure regulation system was employed to maintain a constant gas density of 33 μg/cm^3 (equivalent pressure at room temperature 200 mbar). Constant electric-field electrodes and a two-stage "gutter structure" radiofrequency carpet (RFC) system [50] have been developed

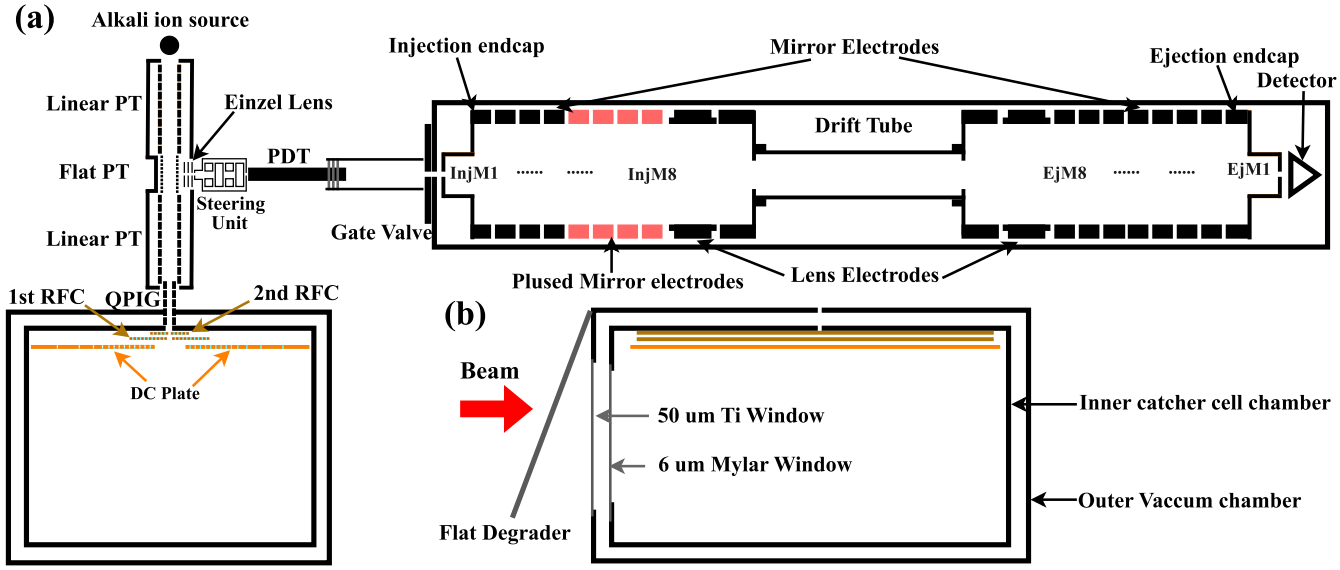

FIG. 1. (a) Schematic view of the ZD-MRTOF experimental setup: cryogenic helium gas-filled catcher cell, ion trap chamber, and MRTOF-MS system shown in the direction of the incoming beam, the red-colored squares in the MRTOF chamber indicate the electrodes which were used for the PMIMS method (see text). (b) Side view of the catcher cell system perpendicular to the incoming beam direction. The DC plate and RF carpets (RFC) in the catcher cell are indicated in orange and brown, respectively.

to transport and extract the ions out of the inner catcher cell chamber. At the first stage RFC, the inhomogeneous RF field, creating an effective force that repels the ions from the electrodes [51], coupled with a static electric field, transported the ions toward the next RFC stage. The second RFC was operated using the ion-surfing mode [52–54]. To this end, the RF field was superimposed with a traveling wave signal (5–100 kHz) in the audiofrequency (AF) spectrum, such that the AF components applied to adjacent electrodes have a 90° phase difference to form a moving potential minimum. The ions were thereby driven to an exit hole with a diameter of 0.65 mm and extracted from the inner catcher cell chamber. Downstream from the inner catcher cell chamber, a segmented quadrupole ion guide (smQPIG), installed inside a differential pumping section, transported the extracted ions to a triplet ion trap chamber [55]. As shown in Fig. 1, the triplet ion trap system contains two linear Paul traps, one on each side of a planar Paul trap (called "flat trap"). The front and rear linear Paul traps independently and simultaneously accept and accumulate analyte ions from the catcher cell and reference ions from a thermal alkali ion source. The ions from the thermal ion source served to correct time-of-flight (TOF) drifts using the concomitant referencing technique [56] and can be employed as reference ions of well-known atomic mass for high-precision mass measurements [57] when no such isobaric ion species are delivered from the gas catcher. As nuclides of well-known atomic masses were included among each isobar chain of the ions of interest in this work, the thermal $^{85}Rb^{+}$ ions (counts rate: 23 per s) were used only for the purpose of drift correction. The analyte and alkali ions were alternately injected into the flat trap [58] in a 50 ms cycle (25 ms each), which allows for excellent tracking of TOF fluctuations. After cooling in the flat trap ($P_{He} \sim 10^{-4}$ mbar), the ions were orthogonally extracted and injected into the MRTOF-MS. The MRTOF-MS is composed of a pair of electrostatic ion mirrors separated by a field-free drift tube region. In the transfer section between the flat trap and MRTOF-MS, a pulsed drift tube adjusts the energy of the ions to reach a mean kinetic energy of 2.5 keV in the field-free central drift tube of the device. The ions were reflected back and forth between the injection and ejection end caps for ≈600 laps to achieve a time focus. Their times of flight, defined as the duration between the flat trap ejection signal and the ion detection at a fast ion-impact detector (MagneTOF), were recorded using a time-to-digital converter (TDC) model MCS6A (Fast ComTec), which has a time resolution of 100 ps. To limit the ions analyzed in any given measurement to a single isobaric chain, the pulsed-mirror in-MRTOF selection (PMiMS) method was used. The usage of this scheme is indicated by highlighting the pulsed mirror electrodes in Fig. 1, and a detailed description can be found in Refs. [14,59]; this method has since been replaced by use of an in-trap deflector [14].

III. DATA ANALYSIS

The TOF peaks of the measured ions drift in unison during the measurements, mainly due to small, random fluctuations in the voltages applied to the electrostatic mirror electrodes and thermal expansion and contraction of the device [60]. The first step of data analysis is to perform a software-based drift correction via time-resolved tracking of the $^{85}Rb^{+}$ TOF peak. Figure 2 shows examples of the $^{85}Rb^{+}$ TOF spectrum before and after drift correction. We note that due to particular difficulties with a voltage channel during this commissioning run, the drifts were more severe than in the usual operation. As shown in Fig. 2(b), after drift correction, the time resolving power reached $R_t = \frac{t}{\Delta t_{FWHM}} \approx 10^6$, corresponding to a mass resolving power of $R_m \approx 5 \times 10^5$. The resulting TOF spectra

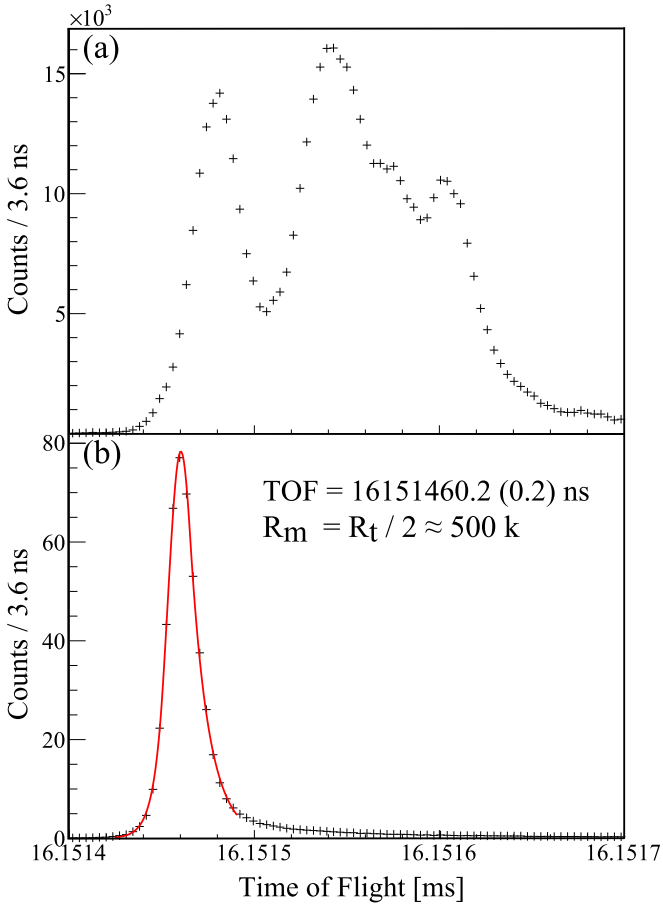

FIG. 2. Time-of-flight spectra for $^{85}Rb^{+}$ ions (a) before and (b) after drift correction. The red line indicates the fitting function (see text).

for the analytes are shown in Fig. 3. In these spectra, Mo and Tc isotopes were provided by the ZD spectrometer. Due to the travel time in the catcher cell, products along the β-decay chain of the precursor isotopes were observed as well.

The second step in the analysis is fitting the peaks to extract the TOFs and their uncertainties. In this work, a Gaussian function coupled with two exponential tails [61] was employed to fit the peaks in the TOF spectra. The definition of the fitting function is shown in Eq. (1),

$$f(t) = A \cdot \begin{cases} \exp\left(\frac{\Delta_L(2t-2t_c+\Delta_L)}{2w^2}\right) & t \leqslant t_L \\ \exp\left(\frac{-(t-t_c)^2}{2w^2}\right) & t_L < t < t_R, \\ \exp\left(\frac{\Delta_R(-2t+2t_c+\Delta_R)}{2w^2}\right) & t \geqslant t_R \end{cases} \quad (1)$$

where A and t_c are the amplitude and maximum position of this function, respectively, w is the width of the central Gaussian part, $t_L(=t_c-\Delta_L)$ and $t_R(=t_c+\Delta_R)$ are the transition points of the left and right side of the Gaussian function, where the Gaussian function changes to an exponential function smoothly for both the function value and the first derivative. The shape of the TOF peaks depends on the settings of ion optics, and in the present case, the fitting results using the function described in Eq. (1) were satisfying (for the use of other Gaussian or exponential-Gaussian hybrid functions, see [62,63]).

First, we determined the parameters of w, t_L, and t_R by fitting the most intense analyte ion peak and then fixed these parameters to fit other peaks in the same TOF spectrum. The maximum-likelihood method was used in the fitting process. The recorded t_c and its uncertainty were used for mass calculation by

$$m = \frac{q}{q_{ref}} m_{ref} \left(\frac{t_c - t_0}{t_c^{ref} - t_0}\right)^2 = \frac{q}{q_{ref}} m_{ref} \rho^2, \quad (2)$$

where q and q_{ref} are the charge state of analyte and reference ions, respectively (in the present work, the charge states of analyte and reference ions are 1^+), and t_0 is the time difference between the start of the TDC and the real ejection pulse timing of the flat ion trap (see [64] for a dedicated investigation). The t_0 was fixed at a premeasured value of 130 ns in this work; through the use of isobaric mass references, the mass uncertainty contribution from variations of t_0 becomes negligible [63]. We have determined the masses of the analyte ions using a reference species of well-known atomic mass and high abundance in each PMiMS-purified isobaric chain. Here, ^{111}Tc [ME: $-69025(11)\,\mathrm{keV}/c^2$] [35], ^{112}Tc [ME : $-65259(6)\,\mathrm{keV}/c^2$] [35], and ^{113}Tc [ME : $-62812(3)\,\mathrm{keV}/c^2$] [22] (see in Table I), having accurately measured precise atomic masses, were used as reference ions.

The mass uncertainties of the analyte species were directly obtained from the uncertainties of m_{ref}, t_c, and t_c^{ref}. AME2020 offers the uncertainties of m_{ref}, and the statistical errors of t_c and t_c^{ref} were obtained in the fitting process.

As a crosscheck, the double-references method, in which the t_0 term is eliminated by using of a second reference mass from the spectrum, was used for comparison in the present analysis. The analyte ion mass as a function of two input masses is described as [13]

$$m = \left(C(\sqrt{m_{ref1}} - \sqrt{m_{ref2}}) + \frac{\sqrt{m_{ref1}} + \sqrt{m_{ref2}}}{2}\right)^2, \quad (3)$$

where $C = (2t_c - t_c^{ref1} - t_c^{ref2})/(2(t_c^{ref1} - t_c^{ref2}))$. This method has been employed using another well-known species (^{111}Rh, ^{112}Ru, and ^{113}Ru) in the spectrum and the Tc isotopes as mentioned before. The results of both analyses agreed within the 1-σ uncertainty band. However, due to the additional error terms involved, the double-reference analysis produces noticeably greater mass uncertainties. As such, we use the single-reference method to determine the atomic mass values reported herein.

IV. RESULTS AND DISCUSSION

The mass excess values determined in this work are listed in Table I. Figure 4 illustrates the comparison between the present results and the literature data. A good agreement between our results and the previous precisely measured mass values from AME2020 is observed. In the two cases of ^{111}Ag and ^{111}Pd, the deviation from the AME2020 data is above one standard deviation, but agrees within 2-σ. For ^{113}Ru, the mass

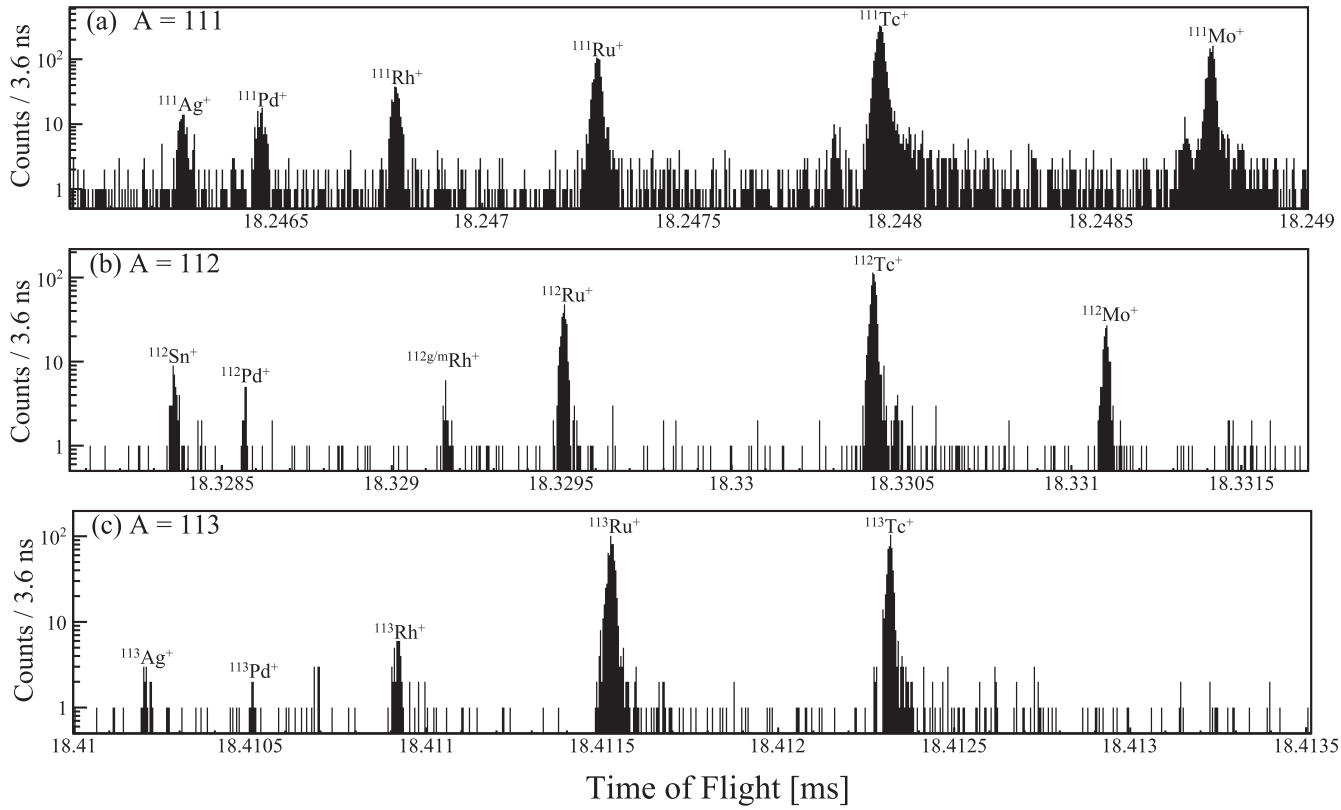

FIG. 3. Time-of-flight spectra of A/q = 111 (a), 112 (b), and 113 (c), for 600 laps. The most intense peaks in each spectrum (^{111}Tc$^+$, ^{112}Tc$^+$, and ^{113}Ru$^+$) were used to determine the fit shape parameters in the fitting process. The mass resolution was insufficient to resolve the ground and isomeric states of ^{112}Rh.

uncertainty was reduced from the previous value of 38 keV to 7 keV. In the case of ^{112}Mo [half life: 125(5) ms, count rate: 155 per h], the mass excess value is determined to be −57470 (8) keV, and matches very well with the extrapolated mass excess value in AME2020. For ^{112}Rh, the mass resolution is insufficient to resolve ground state and isomer, but

TABLE I. Ion species of analyte and reference ions, mass ratio ρ^2 for mass calibration, measured mass excess ME_{MRTOF}, mass excess from the AME2020 ME_{AME2020}, mass deviation calculated as $\Delta m = ME_{\mathrm{MRTOF}} - ME_{\mathrm{AME2020}}$, half-lives of analyte ions, and the total number of the detected ions N_{ion} in this work. The half-lives of $^{111-113}$Tc are 350(21) ms [65], 271(15) ms [5], and 152(8) ms, respectively.

Species	Ref. ion	ρ^2	ME_{MRTOF} (keV/c^2)	ME_{AME2020} (keV/c^2)	Δm (keV/c^2)	Half-lives	N_{ion} (Counts)
^{111}Ag	^{111}Tc	0.99981448(12)	−88194(17)	−88215(1) [66]	21(17)	7.43(1) d [67]	115
^{111}Pd	^{111}Tc	0.99983558(11)	−86014(15)	−85986(1) [68]	−28(15)	23.56(9) min [69]	125
^{111}Rh	^{111}Tc	0.999871359(73)	−82317(13)	−82304(7) [35]	−13(15)	11(1) s	262
^{111}Ru	^{111}Tc	0.999924856(45)	−76789(12)	−76785(10) [35]	−4(16)	2.12(7) s	743
^{111}Mo	^{111}Tc	1.000087920(37)	−59940(11)	−59940(13) [22]	0(17)	193.6(44) ms [5]	1300
^{112}Sn	^{112}Tc	0.99977548(13)	−88667(15)	−88655.1(0.3) [70]	−11.9(15.0)	stable	83
^{112}Pd	^{112}Tc	0.99979797(22)	−86323(24)	−86321(7) [35]	−2(25)	21.04(17) h	34
$^{112g/m}$Rh [a]	^{112}Tc	0.99986265(17)	−79579(18)	−79730(40) [35,71]	151(44)	*g*: 3.4(4) s [72] *m*: 6.73(15) s [72]	40
^{112}Ru	^{112}Tc	0.999900557(50)	−75627(8)	−75631(10) [35]	4(13)	1.75(7) s	493
^{112}Mo	^{112}Tc	1.000074708(61)	−57470(8)	−57480(200)[b]	–	125(5) ms [5]	283
^{113}Ag	^{113}Tc	0.99977011(38)	−86995(41)	−87027(17) [73]	32(44)	5.37(5) h	16
^{113}Pd	^{113}Tc	0.99980262(45)	−83575(48)	−83591(7) [35]	16(48)	93(5) s	18
^{113}Rh	^{113}Tc	0.99984817(15)	−78783(16)	−78767(7) [35]	−16(17)	2.80(12) s [74]	80
^{113}Ru	^{113}Tc	0.999913924(56)	−71866(7)	−71868(38) [35,75]	2(39)	0.80(5) s	1051

[a]The resolving power is insufficient to resolve the states.
[b]Extrapolated values of AME2020.

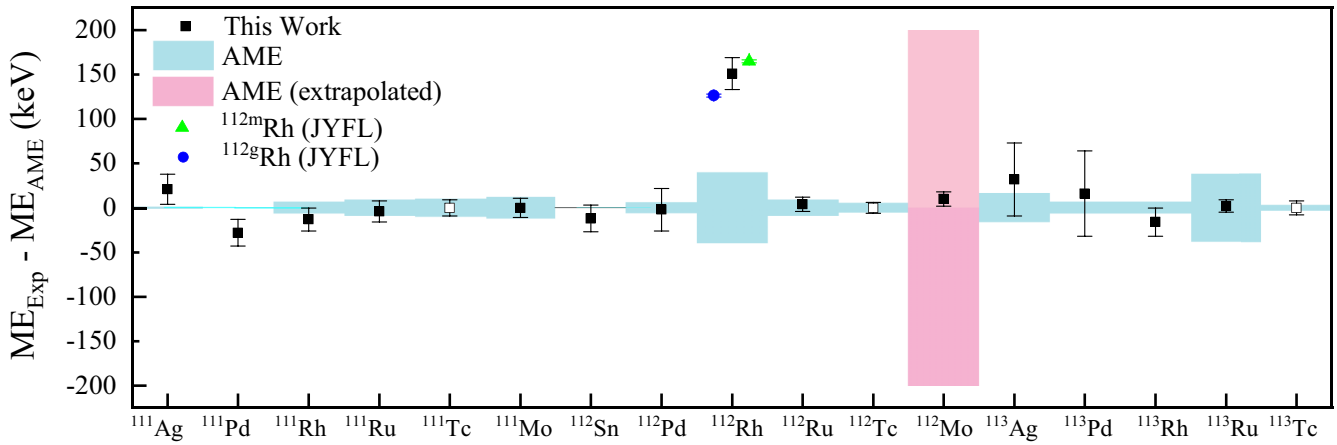

FIG. 4. Mass deviations between our results and the values listed in AME2020. Open symbol indicates species which have been used as reference ions for the fitting process and mass calculation. The blue gray bands indicate the experimental uncertainties from AME2020 and the pink band indicates the extrapolated mass uncertainties. The mass values of ^{112m}Rh (green triangle) and ^{112g}Ru (blue circle) are taken from Ref. [36].

the mass excess value is determined to be −79579 (18) keV, the deviation between the present result and AME2020 is 151 (44) keV. However, our result agrees well with the mass excess value −79577 (8) keV listed in Ref. [35]. The latter value was measured by the JYFLTRAP Penning trap. In more recent work, Hukkanen *et al.* [36] have determined the mass excess of the ground state of ^{112}Rh to be −79603.7 (17) keV, and an isomer [half life: 6.73(15) s] at 38.4 (19) keV has been measured—our value falls squarely between them, as would be expected for an unresolved admixture of states.

We illustrate the mass surface of this region addressed in Figs. 5 and 6, where the two-neutron separation energies $S_{2n}(N, Z) = m(N-2, Z) - m(N, Z) + 2m_n$ from Zr to Ag, and the two-neutron empirical shell gaps $\delta_{2n}(N, Z) = S_{2n}(N, Z) - S_{2n}(N+2, Z)$ for Mo isotopes including the new data point are shown. Hereby, $m(N, Z)$ is the atomic mass of a nucleus with Z protons and N neutrons, and m_n is the mass of a neutron. The S_{2n} value will decrease approximately linearly with increasing neutron number along an isotopic chain, and a sharp drop is observed when crossing the nuclear shell closures or subshell closures. The variations of S_{2n} and δ_{2n} are not generally sensitive to nuclear shape transitions, but show discontinuities in the trend in cases where the binding energy of the system is significantly affected, as known for transitions from spherical to deformed.

A prominent onset of nuclear deformation is observed around $N = 60$ below the molybdenum isotopes with a clear signature in the S_{2n} values. For the Mo isotopic chain,

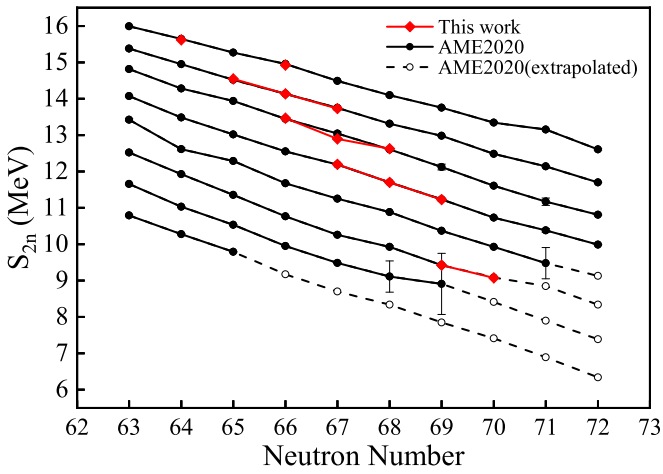

FIG. 5. Two-neutron separation energies for isotopic chains from Zr to Ag. The values from this work and AME2020 are in red and black marks, respectively. Extrapolated values from trends of the mass surface (TMS, see AME2020) are shown with open circles.

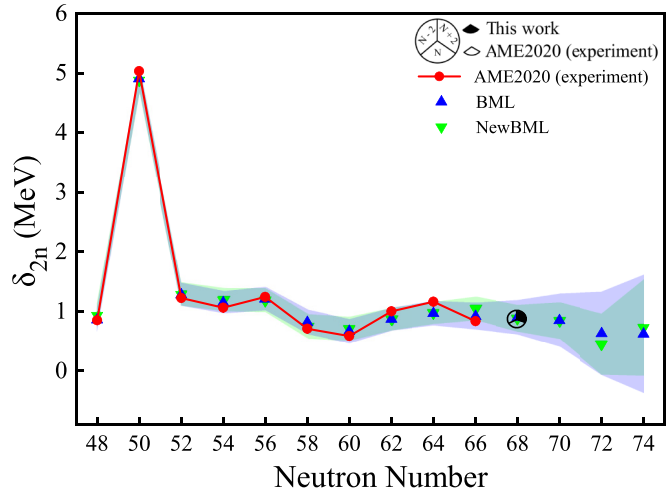

FIG. 6. Plot of the empirical shell gap δ_{2n} for even-even Mo isotopes. The δ_{2n} calculated with the AME2020 values are shown with red circles. At $N = 68$, the data point is divided into three parts to indicate the mass data used for δ_{2n} calculations [$N-2 : m(N-2, Z)$, $N : m(N, Z)$, $N+2 : m(N+2, Z)$]. Black indicates the data from this work, while white indicates the experimental values from AME2020. The δ_{2n} predictions of BML [80] and NewBML (see text) are shown with blue and green marks. Uncertainties are indicated by shaded bands.

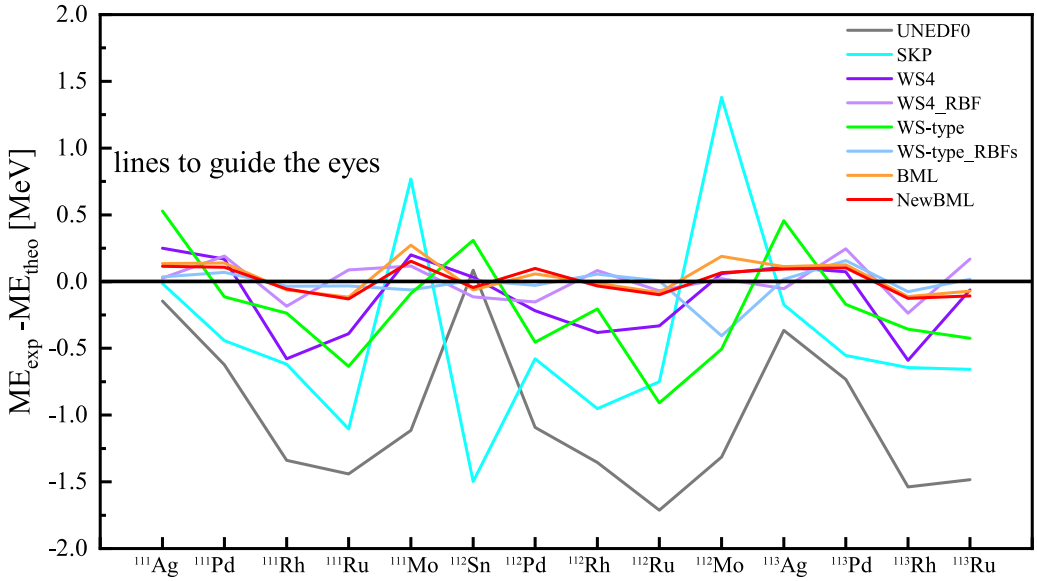

FIG. 7. Comparison of experimental masses with different theoretical values. In the case of ^{112}Rh, we compare to the ^{112g}Rh value in [36] based on our confirmation of their measurement. The different color lines are used to guide the eyes.

the shape coexistence has been identified in ^{106,108,110}Mo, suggesting prolate ground states and triaxial bands [33]. Conversely, the covariant density functional theory (CDFT) calculations for the ground states in the molybdenum isotopes show large β_2 deformation parameters with triaxial shapes for $N = 62$–66, which then turn back to lower deformation parameters with oblate shapes for $N = 68$–70 [34]. In Fig. 6, no exceptional behavior in the δ_{2n} trend from ^{108}Mo to ^{110}Mo is observed, the predicted shape transition from triaxial to oblate is not present. A more sensitive indicator for ground state nuclear deformation, as obtained in the safe Coulomb excitation experiments with ^{96,98}Sr [23], and lifetime measurements [20,33] would be needed for ^{112}Mo to study shape transition and coexistence. As shown in Fig. 5, this region's general trend of S_{2n} values is strikingly smooth, and no exceptional S_{2n} behavior has been detected at $N = 70$. For the study of shell stabilization at $N = 70$, precision mass values of more neutron-rich nuclides would be necessary.

A comparison of various theoretical models and the measured masses of isotopes presented in this work is shown in Fig. 7. The root mean square (rms) deviations have been calculated to be 1150 keV, 827 keV, 306 keV, 143 keV, 442 keV, 122 keV, and 127 keV for UNEDF0 [76], SKP [77], WS4 [78], WS4_RBF [78], WS-type [79], WS-type_RBFs [79], and BML [80], respectively. Of particular interest, by using machine learning to study the mass surface of even-even nuclei and the correlation energies to their neighboring nuclei with Bayesian neural networks, the Bayesian machine learning (BML) model achieved an accuracy of about 100 keV in the experimentally known region, which is a better performance than achieved with other machine learning methods in the region of interest. Since the BML model includes the known physics in various sophisticated mass models, it properly evaluates the uncertainties of mass predictions even for nuclei far from the known region [80]. Therefore, in this work, we employ the BML model to study the impact of new measurements on nuclear mass prediction. By including the newly measured mass of ^{112}Mo as training data, the updated BML (NewBML) model improves not only the mass description of ^{112}Mo alone but also the overall mass description in this region. The theoretical predictions of the NewBML model show an improved agreement with our results, with a rms deviation of only 101 keV. To show the influence of the new ^{112}Mo mass data on the extrapolated masses using the BML model, the δ_{2n} of Mo isotopes predicted by NewBML are shown together with the experimental values in Fig. 6. It is found that the new mass slightly changes the trend of the extrapolation for NewBML, and reduces the uncertainties of the δ_{2n} extrapolations, especially for isotopes with $N > 70$. The result demonstrates the importance of the new mass measurement for mass extrapolation towards more exotic isotopes. Furthermore, with the mass values predicted by the NewBML model, there is no shell stability at $N = 70$ until the very neutron-rich region, a result that remains to be confirmed by measurements in future studies.

V. SUMMARY

Using the ZD MRTOF-MS system, we have measured the masses of ^{111,113}Ag, $^{111-113}$Pd, $^{111-113}$Rh, $^{111-113}$Ru, and ^{111,112}Mo during the third of four commissioning experiments for the device, performed commensal to in-beam γ-ray spectroscopy measurements. The mass of ^{112}Mo [mass excess: $-57470\,(8)$ keV] has been directly measured. The atomic mass of ^{112}Rh determined by the JYFLTRAP group [35,36], previously excluded by the Atomic Mass Evaluation, has been confirmed. In general, a good agreement has been observed between our results and the AME2020. The mass resolving power reached $\approx 5 \times 10^5$ in this work. The success of these online commissioning experiments proves the reliability of the ZD MRTOF-MS system. Combined with the mass values from AME2020 and our results, we have studied the

two-neutron separation energy and neutron shell gap in the context of recent theoretical calculations for nuclear shapes in the mass region of $A = 110$. From these data, we conclude that up to ^{112}Mo, there is no stabilizing shell effect corresponding to the harmonic oscillator gap at N = 70. Studying the shell evolution requires more data toward the neutron drip-line. The data were compared to state-of-the-art mass models and included in new calculations of a Bayesian machine learning mass model, showing an improvement in the predictive power using new data.

ACKNOWLEDGMENTS

We express our gratitude to the RIKEN Nishina Center for Accelerator-Based Science and the Center for Nuclear Science at Tokyo University for their support of the online experiments. We thank the HiCARI collaboration for sharing the beam time. Thanks to the Institute of Modern Physics and the China Scholarship Council for their support of D.S.H.. This work was supported by the Japan Society for the Promotion of Science KAKENHI (Grants No. 2200823, No. 24224008, No. 24740142, No. 15H02096, No. 15K05116, No. 17H01081, No. 17H06090, No. 18K13573, No. 18H05462, No. 19H00679, No. 19H05145, No. 19K14750, No. 20H05648, No. 21H00117, No. 21K13951, No. 22H01257, and No. 22H04946), RIKEN Junior Research Associate Program, the RIKEN program for Evolution of Matter in the Universe (r-EMU), RIKEN International Nuclear Astrophysics Network (RiNA-Net), the UK STFC Grant No. ST/P003885/1, the Royal Society, and Research Grants Council (RGC) of Hong Kong (GRF-17312522), and the National Natural Science Foundation of China (Grants No.11961141004 and No. 12135004), the Strategic Priority Research Program of Chinese Academy of Sciences (Grant No. XDB34010000), and the National Key Research and Development Program of China (Contract No. 2018YFA0404402).

[1] D. Lunney, J. M. Pearson, and C. Thibault, Rev. Mod. Phys. **75**, 1021 (2003).
[2] S. Goriely, N. Chamel, and J. M. Pearson, Phys. Rev. C **88**, 024308 (2013).
[3] H. Schatz, Int. J. Mass Spectrom. **349–350**, 181 (2013).
[4] M. R. Mumpower, R. Surman, G. C. McLaughlin, and A. Aprahamian, Prog. Part. Nucl. Phys. **86**, 86 (2016).
[5] G. Lorusso, S. Nishimura, Z. Y. Xu, A. Jungclaus, Y. Shimizu, G. S. Simpson, P.-A. Söderström, H. Watanabe, F. Browne, P. Doornenbal, G. Gey, H. S. Jung, B. Meyer, T. Sumikama, J. Taprogge, Z. Vajta, J. Wu, H. Baba, G. Benzoni, K. Y. Chae *et al.*, Phys. Rev. Lett. **114**, 192501 (2015).
[6] S. Nishimura, Z. Li, H. Watanabe, K. Yoshinaga, T. Sumikama, T. Tachibana, K. Yamaguchi, M. Kurata-Nishimura, G. Lorusso, Y. Miyashita, A. Odahara, H. Baba, J. S. Berryman, N. Blasi, A. Bracco, F. Camera, J. Chiba, P. Doornenbal, S. Go, T. Hashimoto *et al.*, Phys. Rev. Lett. **106**, 052502 (2011).
[7] T. Sumikama, K. Yoshinaga, H. Watanabe, S. Nishimura, Y. Miyashita, K. Yamaguchi, K. Sugimoto, J. Chiba, Z. Li, H. Baba, J. S. Berryman, N. Blasi, A. Bracco, F. Camera, P. Doornenbal, S. Go, T. Hashimoto, S. Hayakawa, C. Hinke, E. Ideguchi *et al.*, Phys. Rev. Lett. **106**, 202501 (2011).
[8] G. Münzenberg, H. Geissel, and Y. A. Litvinov, AIP Conf. Proc. **1224**, 28 (2010).
[9] H. Wollnik and A. Casares, Int. J. Mass Spectrom. **227**, 217 (2003).
[10] P. Schury, M. Wada, Y. Ito, S. Naimi, T. Sonoda, H. Mita, A. Takamine, K. Okada, H. Wollnik, S. Chon, H. Haba, D. Kaji, H. Koura, H. Miyatake, K. Morimoto, K. Morita, and A. Ozawa, Nucl. Instrum. Methods Phys. Res. B **317**, 537 (2013).
[11] Y. Ishida, M. Wada, and H. Wollnik, Nucl. Instrum. Methods Phys. Res. B **241**, 983 (2005).
[12] R. Wolf, F. Wienholtz, D. Atanasov, D. Beck, K. Blaum, C. Borgmann, F. Herfurth, M. Kowalska, S. Kreim, Y. A. Litvinov, D. Lunney, V. Manea, D. Neidherr, M. Rosenbusch, L. Schweikhard, J. Stanja, and K. Zuber, Int. J. Mass Spectrom. **349–350**, 123 (2013).
[13] F. Wienholtz, D. Beck, K. Blaum, C. Borgmann, M. Breitenfeldt, R. B. Cakirli, S. George, F. Herfurth, J. D. Holt, M. Kowalska, S. Kreim, D. Lunney, V. Manea, J. Menéndez, D. Neidherr, M. Rosenbusch, L. Schweikhard, A. Schwenk, J. Simonis, J. Stanja *et al.*, Nature (London) **498**, 346 (2013).
[14] M. Rosenbusch, M. Wada, S. Chen, A. Takamine, S. Iimura, D. Hou, W. Xian, S. Yan, P. Schury, Y. Hirayama, Y. Ito, H. Ishiyama, S. Kimura, T. Kojima, J. Lee, J. Liu, S. Michimasa, H. Miyatake, J. Y. Moon, M. Mukai *et al.*, Nucl. Instrum. Methods Phys. Res. A **1047**, 167824 (2023).
[15] J. Dobaczewski, I. Hamamoto, W. Nazarewicz, and J. A. Sheikh, Phys. Rev. Lett. **72**, 981 (1994).
[16] B. Pfeiffer, K. L. Kratz, J. Dobaczewski, and P. Möller, Acta Phys. Pol. B **27**, 475 (1996).
[17] K. L. Kratz, B. Pfeiffer, O. Arndt, S. Hennrich, and A. Wöhr, Eur. Phys. J. A **25**, 633 (2005).
[18] N. Paul, A. Corsi, A. Obertelli, P. Doornenbal, G. Authelet, H. Baba, B. Bally, M. Bender, D. Calvet, F. Château, S. Chen, J.-P. Delaroche, A. Delbart, J.-M. Gheller, A. Giganon, A. Gillibert, M. Girod, P.-H. Heenen, V. Lapoux, J. Libert *et al.*, Phys. Rev. Lett. **118**, 032501 (2017).
[19] A. Jungclaus, L. Cáceres, M. Górska, M. Pfützner, S. Pietri, E. Werner-Malento, H. Grawe, K. Langanke, G. Martínez-Pinedo, F. Nowacki, A. Poves, J. J. Cuenca-García, D. Rudolph, Z. Podolyak, P. H. Regan, P. Detistov, S. Lalkovski, V. Modamio, J. Walker, P. Bednarczyk *et al.*, Phys. Rev. Lett. **99**, 132501 (2007).
[20] F. Browne, A. M. Bruce, T. Sumikama, I. Nishizuka, S. Nishimura, P. Doornenbal, G. Lorusso, P. A. Söderström, H. Watanabe, R. Daido, Z. Patel, S. Rice, L. Sinclair, J. Wu, Z. Y. Xu, A. Yagi, H. Baba, N. Chiga, R. Carroll, F. Didierjean *et al.*, Phys. Lett. B **750**, 448 (2015).
[21] D. Atanasov, P. Ascher, K. Blaum, R. B. Cakirli, T. E. Cocolios, S. George, S. Goriely, F. Herfurth, H.-T. Janka, O. Just, M. Kowalska, S. Kreim, D. Kisler, Y. A. Litvinov, D. Lunney, V. Manea, D. Neidherr, M. Rosenbusch, L. Schweikhard, A. Welker *et al.*, Phys. Rev. Lett. **115**, 232501 (2015).

[22] J. Hakala, R. Rodríguez-Guzmán, V. V. Elomaa, T. Eronen, A. Jokinen, V. Kolhinen, I. Moore, H. Penttilä, M. Reponen, J. Rissanen *et al.*, Eur. Phys. J. A **47**, 129 (2011).

[23] E. Clément, M. Zielińska, A. Görgen, W. Korten, S. Péru, J. Libert, H. Goutte, S. Hilaire, B. Bastin, C. Bauer, A. Blazhev, N. Bree, B. Bruyneel, P. A. Butler, J. Butterworth, P. Delahaye, A. Dijon, D. T. Doherty, A. Ekström, C. Fitzpatrick *et al.*, Phys. Rev. Lett. **116**, 022701 (2016).

[24] T. Togashi, Y. Tsunoda, T. Otsuka, and N. Shimizu, Phys. Rev. Lett. **117**, 172502 (2016).

[25] C. Sotty, M. Zielińska, G. Georgiev, D. L. Balabanski, A. E. Stuchbery, A. Blazhev, N. Bree, R. Chevrier, S. Das Gupta, J. M. Daugas, T. Davinson, H. De Witte, J. Diriken, L. P. Gaffney, K. Geibel, K. Hadyńska-Klęk, F. G. Kondev, J. Konki, T. Kröll, P. Morel *et al.*, Phys. Rev. Lett. **115**, 172501 (2015).

[26] J. Dudouet, A. Lemasson, G. Duchêne, M. Rejmund, E. Clément, C. Michelagnoli, F. Didierjean, A. Korichi, G. Maquart, O. Stezowski, C. Lizarazo, R. M. Pérez-Vidal, C. Andreoiu, G. de Angelis, A. Astier, C. Delafosse, I. Deloncle, Z. Dombradi, G. de France, A. Gadea *et al.*, Phys. Rev. Lett. **118**, 162501 (2017).

[27] S. Naimi, G. Audi, D. Beck, K. Blaum, C. Böhm, C. Borgmann, M. Breitenfeldt, S. George, F. Herfurth, A. Herlert, M. Kowalska, S. Kreim, D. Lunney, D. Neidherr, M. Rosenbusch, S. Schwarz, L. Schweikhard, and K. Zuber, Phys. Rev. Lett. **105**, 032502 (2010).

[28] M. Albers, N. Warr, K. Nomura, A. Blazhev, J. Jolie, D. Mücher, B. Bastin, C. Bauer, C. Bernards, L. Bettermann, V. Bildstein, J. Butterworth, M. Cappellazzo, J. Cederkäll, D. Cline, I. Darby, S. Das Gupta, J. M. Daugas, T. Davinson, H. De Witte *et al.*, Phys. Rev. Lett. **108**, 062701 (2012).

[29] F. Flavigny, P. Doornenbal, A. Obertelli, J.-P. Delaroche, M. Girod, J. Libert, T. R. Rodriguez, G. Authelet, H. Baba, D. Calvet, F. Château, S. Chen, A. Corsi, A. Delbart, J.-M. Gheller, A. Giganon, A. Gillibert, V. Lapoux, T. Motobayashi, M. Niikura *et al.*, Phys. Rev. Lett. **118**, 242501 (2017).

[30] P. Singh, W. Korten, T. W. Hagen, A. Görgen, L. Grente, M.-D. Salsac, F. Farget, E. Clément, G. de France, T. Braunroth, B. Bruyneel, I. Celikovic, O. Delaune, A. Dewald, A. Dijon, J.-P. Delaroche, M. Girod, M. Hackstein, B. Jacquot, J. Libert *et al.*, Phys. Rev. Lett. **121**, 192501 (2018).

[31] W. Witt, V. Werner, N. Pietralla, M. Albers, A. D. Ayangeakaa, B. Bucher, M. P. Carpenter, D. Cline, H. M. David, A. Hayes, C. Hoffman, R. V. F. Janssens, B. P. Kay, F. G. Kondev, W. Korten, T. Lauritsen, O. Möller, G. Rainovski, G. Savard, D. Seweryniak *et al.*, Phys. Rev. C **98**, 041302(R) (2018).

[32] T. Otsuka and Y. Tsunoda, J. Phys. G: Nucl. Part. Phys. **43**, 024009 (2016).

[33] J. Ha, T. Sumikama, F. Browne, N. Hinohara, A. M. Bruce, S. Choi, I. Nishizuka, S. Nishimura, P. Doornenbal, G. Lorusso, P.-A. Söderström, H. Watanabe, R. Daido, Z. Patel, S. Rice, L. Sinclair, J. Wu, Z. Y. Xu, A. Yagi, H. Baba *et al.*, Phys. Rev. C **101**, 044311 (2020).

[34] P. Kumar, V. Thakur, S. Thakur, V. Kumar, and S. K. Dhiman, Eur. Phys. J. A **57**, 36 (2021).

[35] U. Hager, V.-V. Elomaa, T. Eronen, J. Hakala, A. Jokinen, A. Kankainen, S. Rahaman, S. Rinta-Antila, A. Saastamoinen, T. Sonoda, and J. Äystö, Phys. Rev. C **75**, 064302 (2007).

[36] M. Hukkanen, W. Ryssens, P. Ascher, M. Bender, T. Eronen, S. Grévy, A. Kankainen, M. Stryjczyk, L. Al Ayoubi, S. Ayet, O. Beliuskina, C. Delafosse, W. Gins, M. Gerbaux, A. Husson, A. Jokinen, D. A. Nesterenko, I. Pohjalainen, M. Reponen, S. Rinta-Antila *et al.*, Phys. Rev. C **107**, 014306 (2023).

[37] M. Wang, W. Huang, F. Kondev, G. Audi, and S. Naimi, Chin. Phys. C **45**, 030003 (2021).

[38] K. Wimmer, P. Doornenbal, N. Aoi, H. Baba, F. Browne, P. Campell, H. Crawford, H. De Witte, C. Fransen, H. Hess, S. Iwazaki, J. Kim, A. Kohda, T. Koiwai, B. Mauss, B. Moon, T. Parry, P. Reiter, D. Suzuki, R. Taniuchi *et al.*, RIKEN Acc. Prog. Rep. **54**, S27 (2021).

[39] P. Doornenbal, K. Wimmer, N. Aoi, H. Baba, F. Browne, P. Campell, M. Carpenter, A. Corsi, M. L. Cortéz, H. Crawford, M. Cromaz, P. Fallon, A. Gillibert, H. Hess, E. Ideguchi, V. Isobe, T. ans Lapoux, H. Liu, A. Macchiavelli, M. Niikura, O. Möller *et al.*, RIKEN RIBF Proposal No. 1812-ribf173 (2018).

[40] Y. Yano, Nucl. Instrum. Methods Phys. Res. B **261**, 1009 (2007).

[41] H. Sakurai, Nucl. Phys. A **805**, 526c (2008).

[42] T. Kubo, Nucl. Instrum. Methods Phys. Res. B **204**, 97 (2003).

[43] T. Kubo, D. Kameda, H. Suzuki, N. Fukuda, H. Takeda, Y. Yanagisawa, M. Ohtake, K. Kusaka, K. Yoshida, N. Inabe, T. Ohnishi, A. Yoshida, K. Tanaka, and Y. Mizoi, Prog. Theor. Exp. Phys. **2012**, 1, 03C003 (2012).

[44] A. Takamine, S. Iimura, M. Rosenbusch, M. Wada, S. Chen, J. Liu, P. Schury, T. Sonoda, T. M. Kojima, I. Katayama, Y. X. Watanabe, H. Ueno, and H. Ishiyama, RIKEN Acc. Prog. Rep. **53**, 108 (2020).

[45] A. Takamine, S. Iimura, D. Hou, M. Wada, M. Rosenbusch, S. Chen, W. Xian, S. Yan, P. Schury, Y. Ito, T. M. Kojima, T. Sonoda, Y. X. Watanabe, H. Ueno, and H. Ishiyama, RIKEN Acc. Prog. Rep. **54**, 93 (2021).

[46] M. Rosenbusch, M. Wada, P. Schury, Y. Ito, H. Ishiyama, S. Ishizawa, Y. Hirayama, S. Kimura, T. M. Kojima, H. Miyatake, J. Y. Moon, T. Niwase, T. Sonoda, A. Takamine, Y. X. Watanabe, and H. Wollnik, Nucl. Instrum. Methods Phys. Res. B **463**, 184 (2020).

[47] S. Chen, Y. Hirayama, D. Hou, S. Iimura, H. Ishiyama, Y. Ito, S. Kimura, J. Liu, H. Miyatake, S. Nishimura, T. Niwase, M. Rosenbusch, P. Schury, A. Takamine, M. Wada, Y. X. Watanabe, H. Wollnik, W. Xian, and S. Yan, RIKEN Accel. Prog. Rep. **54**, 97 (2021).

[48] P. Schury, M. Wada, Y. Ito, D. Kaji, H. Haba, Y. Hirayama, S. Kimura, H. Koura, M. MacCormick, H. Miyatake, J. Y. Moon, K. Morimoto, K. Morita, I. Murray, A. Ozawa, M. Rosenbusch, M. Reponen, A. Takamine, T. Tanaka, Y. X. Watanabe *et al.*, Nucl. Instrum. Methods Phys. Res. B **407**, 160 (2017).

[49] D. J. Morrissey, G. Bollen, M. Facina, and S. Schwarz, Nucl. Instrum. Methods Phys. Res. B **266**, 4822 (2008).

[50] A. Takamine, M. Rosenbusch, M. Wada, P. Schury, J. Y. Moon, T. Sonoda, T. M. Kojima, I. Katayama, Y. X. Watanabe, H. Ueno, and H. Ishiyama, RIKEN Acc. Prog. Rep. **52**, 139 (2019).

[51] M. Wada, Y. Ishida, T. Nakamura, Y. Yamazaki, T. Kambara, H. Ohyama, Y. Kanai, T. M. Kojima, Y. Nakai, N. Ohshima, A. Yoshida, T. Kubo, Y. Matsuo, Y. Fukuyama, K. Okada, T. Sonoda, S. Ohtani, K. Noda, H. Kawakami, and I. Katayama, Nucl. Instrum. Methods Phys. Res. B **204**, 570 (2003).

[52] S. Masuda, K. Fujibayashi, K. Ishida, and H. Inaba, IEEJ Trans. Electr. **92**, 9 (1972).

[53] G. Bollen, Int. J. Mass Spectrom. **299**, 131 (2011).

[54] F. Arai, Y. Ito, M. Wada, P. Schury, T. Sonoda, and H. Mita, Int. J. Mass Spectrom. **362**, 56 (2014).
[55] Y. Ito, P. Schury, M. Wada, S. Naimi, C. Smorra, T. Sonoda, H. Mita, A. Takamine, K. Okada, A. Ozawa, and H. Wollnik, Nucl. Instrum. Methods Phys. Res. B **317**, 544 (2013).
[56] P. Schury, Y. Ito, M. Rosenbusch, H. Miyatake, M. Wada, and H. Wollnik, Int. J. Mass Spectrom. **433**, 40 (2018).
[57] L. Nies, D. Atanasov, M. Athanasakis-Kaklamanakis, M. Au, K. Blaum, J. Dobaczewski, B. S. Hu, J. D. Holt, J. Karthein, I. Kulikov, Y. A. Litvinov, D. Lunney, V. Manea, T. Miyagi, M. Mougeot, L. Schweikhard, A. Schwenk, K. Sieja, and F. Wienholtz, Phys. Rev. Lett. **131**, 022502 (2023).
[58] Y. Ito, P. Schury, M. Wada, F. Arai, H. Haba, Y. Hirayama, S. Ishizawa, D. Kaji, S. Kimura, H. Koura, M. MacCormick, H. Miyatake, J. Y. Moon, K. Morimoto, K. Morita, M. Mukai, I. Murray, T. Niwase, K. Okada, A. Ozawa *et al.*, Phys. Rev. Lett. **120**, 152501 (2018).
[59] S. Yan, M. Rosenbusch, W. Xian, S. Chen, Y. Hirayama, D. Hou, S. Iimura, H. Ishiyama, Y. Ito, S. Kimura, J. Liu, H. Miyatake, S. Nishimura, T. Niwase, P. Schury, A. Takamine, M. Wada, Y. X. Watanabe, and H. Wollnik, RIKEN Accel. Prog. Rep. **54**, S28 (2021).
[60] B. Liu, M. Brodeur, D. Burdette, J. Kelly, T. Kim, J. Long, and P. O'Malley, Nucl. Instrum. Methods Phys. Res. A **985**, 164679 (2021).
[61] M. Rosenbusch, Y. Ito, P. Schury, M. Wada, D. Kaji, K. Morimoto, H. Haba, S. Kimura, H. Koura, M. MacCormick, H. Miyatake, J. Y. Moon, K. Morita, I. Murray, T. Niwase, A. Ozawa, M. Reponen, A. Takamine, T. Tanaka, and H. Wollnik, Phys. Rev. C **97**, 064306 (2018).
[62] P. Schury, M. Wada, Y. Ito, F. Arai, S. Naimi, T. Sonoda, H. Wollnik, V. A. Shchepunov, C. Smorra, and C. Yuan, Nucl. Instrum. Methods Phys. Res. B **335**, 39 (2014).
[63] Y. Ito, P. Schury, M. Wada, S. Naimi, T. Sonoda, H. Mita, F. Arai, A. Takamine, K. Okada, A. Ozawa, and H. Wollnik, Phys. Rev. C **88**, 011306(R) (2013).
[64] M. Rosenbusch, P. Schury, M. Wada, S. Iimura, Y. Ito, and H. Wollnik, Int. J. Mass Spectrom. **456**, 116346 (2020).
[65] J. Pereira, S. Hennrich, A. Aprahamian, O. Arndt, A. Becerril, T. Elliot, A. Estrade, D. Galaviz, R. Kessler, K.-L. Kratz, G. Lorusso, P. F. Mantica, M. Matos, P. Möller, F. Montes, B. Pfeiffer, H. Schatz, F. Schertz, L. Schnorrenberger, E. Smith *et al.*, Phys. Rev. C **79**, 035806 (2009).
[66] Y. Litvinov, H. Geissel, T. Radon, F. Attallah, G. Audi, K. Beckert, F. Bosch, M. Falch, B. Franzke, M. Hausmann, M. Hellström, T. Kerscher, O. Klepper, H.-J. Kluge, C. Kozhuharov, K. Löbner, G. Münzenberg, F. Nolden, Y. Novikov, W. Quint *et al.*, Nucl. Phys. A **756**, 3 (2005).
[67] S. Collins, A. Harms, and P. Regan, Appl. Radiat. Isot. **108**, 143 (2016).
[68] W. W. Pratt and R. G. Cochran, Phys. Rev. **118**, 1313 (1960).
[69] K. Krane, Appl. Radiat. Isot. **105**, 278 (2015).
[70] S. Rahaman, V.-V. Elomaa, T. Eronen, J. Hakala, A. Jokinen, A. Kankainen, J. Rissanen, J. Suhonen, C. Weber, and J. Äystö, Phys. Rev. Lett. **103**, 042501 (2009).
[71] J. Äystö, C. Davids, J. Hattula, J. Honkanen, K. Honkanen, P. Jauho, R. Julin, S. Juutinen, J. Kumpulainen, T. Lönnroth, A. Pakkanen, A. Passoja, H. Penttilä, P. Taskinen, E. Verho, A. Virtanen, and M. Yoshii, Nucl. Phys. A **480**, 104 (1988).
[72] G. Lhersonneau, J. C. Wang, S. Hankonen, P. Dendooven, P. Jones, R. Julin, and J. Äystö, Phys. Rev. C **60**, 014315 (1999).
[73] B. Fogelberg, Y. Zongyuan, B. Ekstriim, E. Lund, K. Aleklett, and L. Sihver, Z. Naturforsch., A: Phys. Sci. **337**, 251 (1990).
[74] H. Penttilä, T. Enqvist, P. Jauho, A. Jokinen, M. Leino, J. Parmonen, J. Äystö, and K. Eskola, Nucl. Phys. A **561**, 416 (1993).
[75] B. Sun, R. Knöbel, Y. Litvinov, H. Geissel, J. Meng, K. Beckert, F. Bosch, D. Boutin, C. Brandau, L. Chen, I. Cullen, C. Dimopoulou, B. Fabian, M. Hausmann, C. Kozhuharov, S. Litvinov, M. Mazzocco, F. Montes, G. Münzenberg, A. Musumarra *et al.*, Nucl. Phys. A **812**, 1 (2008).
[76] M. Kortelainen, T. Lesinski, J. Moré, W. Nazarewicz, J. Sarich, N. Schunck, M. V. Stoitsov, and S. Wild, Phys. Rev. C **82**, 024313 (2010).
[77] J. Dobaczewski, H. Flocard, and J. Treiner, Nucl. Phys. A **422**, 103 (1984).
[78] N. Wang, M. Liu, X. Z. Wu, and J. Meng, Phys. Lett. B **734**, 215 (2014).
[79] N. N. Ma, H. F. Zhang, X. J. Bao, and H. F. Zhang, Chin. Phys. C **43**, 044105 (2019).
[80] Z. M. Niu and H. Z. Liang, Phys. Rev. C **106**, L021303 (2022).